



Hypoxia endothelial cells-derived exosomes facilitate diabetic wound healing through improving endothelial cell function and promoting M2 macrophages polarization

Peng Cheng^{a,b,1}, Xudong Xie^{a,b,1}, Liangcong Hu^{a,b,1}, Wu Zhou^{a,b,1}, Bobin Mi^{a,b}, Yuan Xiong^{a,b}, Hang Xue^{a,b}, Kunyu Zhang^c, Yuxiao Zhang^c, Yiqiang Hu^{a,b}, Lang Chen^{a,b}, Kangkang Zha^{a,b}, Bin Lv^{a,b}, Ze Lin^{a,b}, Chuanlu Lin^{a,b}, Guandong Dai^d, Yixin Hu^{e,f}, Tengbo Yu^{g,****}, Hankun Hu^{e,f,h,***}, Guohui Liu^{a,b,**}, Yingze Zhang^{a,i,*}

^a Department of Orthopedics, Union Hospital, Tongji Medical College, Huazhong University of Science and Technology, Wuhan, 430022, China

^b Hubei Province Key Laboratory of Oral and Maxillofacial Development and Regeneration, Wuhan, 430022, China

^c School of Biomedical Sciences and Engineering, South China University of Technology, Guangzhou International Campus, Guangzhou, 511442, China

^d Department of Orthopaedics, Pingshan District People's Hospital of Shenzhen, Pingshan General Hospital of Southern Medical University, Shenzhen, Guangdong, 518118, China

^e Hubei Micro-explore Innovative Pharmaceutical Research Co, Ltd, Wuhan, Hubei, 430071, China

^f Suzhou Organ-on-a-Chip System Science and Technology Co, Ltd, Suzhou, Jiangsu, 215000, China

^g Department of Sports Medicine, The Affiliated Hospital of Qingdao University, Qingdao, China

^h Department of Pharmacy, Zhongnan Hospital of Wuhan University, School of Pharmaceutical Sciences, Wuhan University, Wuhan, 430071, China

ⁱ Department of Orthopaedic Surgery, The Third Hospital of Hebei Medical University, NO.139 Ziqiang Road, Shijiazhuang, 050051, China

ARTICLE INFO

Keywords:

Diabetic wound
Hypoxic exosomes
lncHAR1B
KLF4
Macrophage polarization

ABSTRACT

It is imperative to develop and implement newer, more effective strategies to address refractory diabetic wounds. As of now, there is currently no optimal solution for these wounds. Hypoxic human umbilical vein endothelial cells (HUVECs)-derived exosomes have been postulated to promote diabetic wound healing, however, its effect and molecular mechanism need further study. In this study, we aimed to investigate whether hypoxic exosomes enhance wound healing in diabetics. Based on our high-throughput sequencing, differentially expressed lncRNAs (including 64 upregulated lncRNAs and 94 downregulated lncRNAs) were found in hypoxic exosomes compared to normoxic exosomes. Interestingly, lncHAR1B was one of the prominently upregulated lncRNAs in hypoxic exosomes, showing a notable correlation with diabetic wound healing. More specifically, hypoxic exosomes were transmitted to surrounding cells, which resulted in a significant increase in lncHAR1B level, thereby relieving the dysfunction of endothelial cells and promoting the switch from M1 to M2 macrophages under high glucose conditions. Mechanistically, lncHAR1B directly interacted with the transcription factor basic helix-loop-helix family member e23 (BHLHE23), which subsequently led to its binding to the KLF transcription factor 4 (KLF4) and promoted KLF4 expression. In our *in vivo* experiments, the use of hypoxic exosomes-loaded HGM-QCS hydrogels (Gel-H-Exos) resulted in rapid wound healing compared to that of normoxic exosomes-loaded HGM-QCS hydrogels (Gel-N-Exos) and diabetic groups. Consequently, our study provides potentially novel therapeutic approaches aimed at accelerating wound healing and developing a practical exosomes delivery platform.

Peer review under responsibility of KeAi Communications Co., Ltd.

* Corresponding author. Department of Orthopaedic Surgery, The Third Hospital of Hebei Medical University, NO.139 Ziqiang Road, Shijiazhuang, 050051, China.

** Corresponding author. Department of Orthopedics, Union Hospital, Tongji Medical College, Huazhong University of Science and Technology, Wuhan, 430022, China.

*** Corresponding author. Department of Pharmacy, Zhongnan Hospital of Wuhan University, School of Pharmaceutical Sciences, Wuhan University, Wuhan, 430071, China.

**** Corresponding author.

E-mail addresses: ytb8912@163.com (T. Yu), huhankun@whu.edu.cn (H. Hu), liuguohui@hust.edu.cn (G. Liu), drzhangyz@126.com (Y. Zhang).

¹ These authors contributed equally to this paper.

<https://doi.org/10.1016/j.bioactmat.2023.10.020>

Received 3 August 2023; Received in revised form 19 October 2023; Accepted 19 October 2023

2452-199X/© 2023 The Authors. Publishing services by Elsevier B.V. on behalf of KeAi Communications Co. Ltd. This is an open access article under the CC BY-NC-ND license (<http://creativecommons.org/licenses/by-nc-nd/4.0/>).

1. Introduction

Wound healing is characterized as a highly scheduled process involving hemostasis, inflammation, proliferation, and remodeling phases. However, this procedure is disturbed in diabetic wounds, which results in delayed or stalled wound healing [1,2]. As the prevalence of diabetes continues to rise, an increasing number of people will be at risk of developing diabetic wounds. These wounds can cause severe pain, infection, and even necessitate amputation of the foot [1,3,4]. Although wound care management is an established field and has undergone rapid development, the treatment of diabetic wounds remains a serious issue. This challenge arises from increased oxidative stress and inflammation, poor angiogenesis, and subsequent oxygen deprivation [5]. Hence, strategies aimed at the inhibition of excessive and persistent inflammation and the promotion of angiogenesis represent powerful therapeutic approaches for diabetic wounds.

Recently, exosomes, extracellular nanovesicles with diameters ranging from 30 to 150 nm secreted by diverse cells, have garnered significant scientific and clinical interest. These vesicles function as a molecular vehicle that transfers a specific mix of proteins, lipids, and nucleic acids from one cell to another, mediating communication between cells [6,7]. Several studies have shown that exosomes can enhance angiogenesis and/or reduce inflammation mediated by M1 macrophages, thereby facilitating diabetic wound healing [8–10]. For example, Xiong et al. revealed that medical plant-derived exosomes could be beneficial to diabetic wound healing by inducing M2 macrophages polarization to attenuate inflammation [11]. In addition, Chen et al. demonstrated that exosomes from human urine-derived stem cells promoted angiogenesis to accelerate diabetic wound repair [12]. However, the currently reported treatments have failed to coordinate angiogenesis and macrophage polarization simultaneously in diabetic wounds. Several studies revealed that hypoxia preconditioned human umbilical vein endothelial cells (HUVECs)-derived exosomes enhanced angiogenesis in spinal cord repair and fracture [13,14], but there is no relevant research report on its application in the diabetic wound healing. Considering that hypoxia-pretreated cells-derived exosomes have been reported to speed up angiogenesis and promote M2 macrophages polarization [13,15,16], we hypothesized that exosomes derived from hypoxic endothelial cells might facilitate diabetic wound repair by both accelerating angiogenesis and promoting the switch from M1 to M2 macrophages.

Long non-coding RNAs (lncRNAs) are known to influence gene expressions through interactions with microRNAs (miRNAs), as well as mRNAs and some proteins [17]. Furthermore, lncRNAs have been recognized to play important roles in the regulation of cell proliferation, migration, inflammation, apoptosis, and autophagy [18,19]. Considering the capability of exosomes to transmit information, significant focus and interest has been invested into understanding the implications and functions of lncRNAs found in exosomes [20]. For instance, the mesenchymal stem cells (MSCs)-derived exosomal lncRNA H19 has been observed to shorten the wound healing time in diabetic foot ulcers (DFUs) via the miRNA-152-3p/PTEN axis [21]. Similarly, lncRNA KLF3-AS1 in MSCs-derived exosomes accelerated diabetic cutaneous wound healing through stimulating angiogenesis [22]. Additionally, lncRNA-URIDS has been shown to delay diabetic wound healing by targeting plod1 [23]. The above evidence suggests that exosomal lncRNAs might be involved in the development and progress of diabetic wound healing. Thus, we hypothesized that the lncRNAs in hypoxic endothelial cells-derived exosomes may play an essential role in the treatment of diabetic wounds.

However, the common method of exosome administration is injection, which can affect their function due to the rapid clearance rate [24]. On the other hand, diabetic wound repair and regeneration require a relatively long healing time. Herein, it is necessary to develop a biocompatible scaffold that can serve as a sustained release carrier for exosomes to maintain their bioactivity at the diabetic wound area and

further accelerate wound healing. Hydrogel is structurally similar to natural ECM and is considered promising biomaterials for loading drug or cell to treat wounds [25–27]. Previous related studies have found that, the acrylate β -cyclodextrin (Ac- β -CD) and gelatin-based hydrogels have good biocompatibility, cellular adaptability, and the ability to achieve exosome loading, and chitosan has certain antibacterial properties, which is widely used in synthetic antibacterial hydrogels [28,29]. Based on the properties of the above monomer and the need for treatment of the wound healing, we designed a hydrogel (HGM-QCS hydrogel) that is easily mastered and rapidly glued *in vitro*, whose main components include AC- β -CD, gelatin and chitosan. After mixing with the exosome solution, blue light *in vitro* trigger gelformation in situ using a light-based initiator, which conformed to the shape of the wound. This design will facilitate our understanding of how the effective use of the system improves the limitations of current wound defect treatment.

2. Experimental section

2.1. Materials

β -cyclodextrin (b-CD), acryloyl chloride, dimethyl formamide (DMF), triethyl amine (TEA) were purchased from Aladdin. Quaternary ammonium chitosan (S26618) was purchased from Yuanye. Gelatin (G1890) was purchased from Sigma. Phenyl (2,4,6-trimethylbenzoyl) phosphinic Acid Lithium Salt (LAP) was purchased from Tokyo Chemical Industry (TCI).

2.2. Acrylate β -cyclodextrin (Ac- β -CD) synthesis

To a volume of 150 mL of DMF, 10 g of b-CD and 7 mL of TEA were added. After cooling to 0 °C and stirring, 5 ml of acryloyl chloride was added to the mixture. After 6 h of mixing, the trimethylamine hydrochloride was filtered away, and the resulting clear solution was concentrated to roughly 20 ml using vacuum rotary evaporation. The modified cyclodextrin was precipitated by slowly dripping the solution into 600 ml of acetone. Multiple acetone washes and three days of vacuum drying were performed on the precipitate. Using a 1H NMR spectrometer in D₂O (Bruker Advance 400 MHz), the substitution degree (DS) of CD as 1.6 is verified.

2.3. Preparation of hydrogels

Mixture solutions were made by dissolving gelatin, Ac- β -CD, and quaternary ammonium chitosan (QCS) in PBS at 37 °C overnight; the concentrations of gelatin (8 % w/v) and Ac- β -CD (10 % w/v) were held constant, while the concentrations of QCS varied. Then, a 0.05 % (w/v) dose of LAP was added as the initiator. Supramolecular hydrogels were formed by pipetting the mixture into PVC molds at 37 °C, cooling them to 25 °C, and then exposing them to 405 nm blue light (10 mW/cm², 5 min) at 25 °C.

2.4. Scanning electron microscopy (SEM)

The hydrogels were lyophilized for three days after being frozen in liquid nitrogen for 5 min. After the hydrogels were totally dry, they were sliced apart so that the inside morphology could be investigated. The SEM examinations were performed utilizing a ZEISS Merlin® FE-SEM (Carl Zeiss AG, Germany) with an accelerating voltage of 5kV.

2.5. Rheological and uniaxial compression tests

The tests were carried out on a TA Instrument DHR 30 rheometer. The hydrogels were evenly dispersed across the rheometer's top and bottom plates. Time sweeps were captured using 8 mm (plate to plate) in diameter plates with a 1 mm gap size and a strain of 0.1 % with a frequency of 10 Hz. The premade hydrogels ($\phi = 5$ mm, $h = 3$ mm) were

placed in the middle of the plate and subjected to 1 mm/min of compression during the uniaxial compression testing. In order to determine Young's modulus, the initial linear area of the stress-strain curves (strain 15 %) was used.

2.6. Hydrogel swelling test

For 24 h at 37 °C in phosphate-buffered saline (PBS), freshly manufactured hydrogels (200 µL per gel, n = 4) were allowed to swell and then measured. Finally, the samples were blotted to remove any remaining surface liquid before recording their increased mass. After collecting the samples, we lyophilized them and weighed them again to get their dry weight. The following equation was then used to get the mass swelling ratio:

$$\text{Swelling ratio} = \frac{\text{Swollen hydrogel mass}}{\text{Dry hydrogel mass}}$$

2.7. Degradation analysis of hydrogels

1 mL of PBS was added to the produced hydrogels (n = 4 per group). After removal, the samples were given two rinses in DI water to get rid of any lingering salts. The materials were lyophilized for three days after being frozen in liquid nitrogen for 5 min. Each sample's dry mass was determined at a variety of times, and the sample weight percentage was determined using the following formula:

$$\text{Weight percentage (\%)} \text{ on day } t = \frac{\text{Dry mass on day } x}{\text{Dry mass on day } 0} \times 100\%$$

2.8. Cells and cell culture

HUVECs (Human umbilical vein endothelial cells) were grown in a 37 °C humidified chamber with 5 % CO₂ in DMEM/F12 medium (Gibco) with 10 % fetal bovine serum (FBS, Gibco) and 1 % mixture of penicillin-streptomycin (Gibco). Bone marrow-derived macrophages (BMMs) were prepared as described above [30] and then were cultured in α-MEM medium (Gibco) containing 10 % FBS and 30 ng/ml macrophage colony-stimulating factor (M-CSF).

2.9. Isolation, purification and characterization of exosomes

Cells were culture in a 37 °C humidified chamber with 5 % CO₂ and 21 % O₂ or 1 % O₂ with serum-free medium for 24 h. Then, the cell pellet was separated from the supernatant by centrifuging the mixture at 300 × g for 15 min. A centrifugation at 1000 × g for 20 min eliminated any remaining debris and dead cells. After centrifugation at 10,000 × g for 30 min, the collected supernatant was centrifuged at 100,000 g for 70 min to isolate the exosomes. Finally, exosomes were preserved by suspending them in PBS and storing them at –80 °C. Exosome morphology was studied using TEM to further characterize the separated particles. Zeta potentials and sizes of exosomes were measured using NTA, and exosome markers were identified using a Flow NanoAnalyzer and western blotting assay.

2.10. The release profile of Gel-Exos

The Gel-Exos was obtained by mixing 1 µg exosomes with 100 µl HGM-QCS hydrogel with stirring. Then, the moco BCA protein assay kit (Beyotime, China) was used to test the released exosomes from Gel-Exos. Briefly, the above prepared 100 µl Gel-Exos was placed in the upper transwell chamber placed in a 24-well plate, while 100 µl PBS was added in the lower chamber. Then, 10 µl PBS was collected and replaced by 10 µl fresh PBS at 0, 1, 3, 6, 12, 24, 48, 72 h. The content of release exosomes was detected and the released percentage of exosomes was calculated.

2.11. Antibacterial activity evaluation

The *Escherichia coli* (*E. coli*), *Staphylococcus aureus* (*S. aureus*) and Methicillin-resistant *Staphylococcus aureus* (MRSA) were used to test the antibacterial potential of HGM-QCS hydrogel. Briefly, the 50 µL hydrogel were added into a 48-well microplate and subsequently 10 µL bacterial suspensions (10⁶ CFU/mL) were added onto hydrogel surface. After 2 h incubation, the bacterial survivor on the hydrogel surface was re-suspended using 1 mL sterilized PBS buffer solution and was added on the bacterial culture medium to incubate overnight. The bacterial suspension suspended in PBS was used as a control. The bacterial colony plaque was analyzed.

2.12. RNA-seq and analyses

For RNA sequencing, purified RNA from normoxic or hypoxic exosomes was used for library preparation and construction with Ribo-off rRNA Depletion Kit (Catalog NO. MRZG12324, Illumina) and KC-Digital™ Stranded mRNA Library Prep Kit for Illumina® (FC-122-1001) and then quantified and finally sequenced on NovaSeq 6000 sequencer (Illumina) with PE150 model. Raw reads were aligned to the human genome GRCh37/hg19 by STRA software (version 2.5.3a) with default parameters. Differentially expressed lncRNAs were identified through fold change ≥ 2 and P value < 0.01 with the threshold set for up- and down-regulated genes.

2.13. Western blotting

Total protein was extracted using RIPA lysis buffer following the appropriate procedure. After that, proteins were separated on a 10 % SDS-PAGE gel and then transferred to PVDF membranes. PVDF membranes were treated overnight at 4 °C with particular antibodies following a 1-h blocking step with nonfat milk. After being treated with anti-rabbit secondary antibodies for 1 h at room temperature, membranes were washed three times for 10 min in TBS-T. The membranes were treated with chemiluminescent substrate and then imaged using the Bio-rad Image Capture System after being washed three times with TBS-T.

2.14. Quantitative real-time PCR (qRT-PCR)

TRIzol reagents (Thermo Fisher) were used to extract total RNA from the cells or exosomes. First-strand cDNA was generated with random primers using a PrimeScript™ RT reagent Kit (YEASEN). Then, quantitative real-time PCR was performed using a Hieff® qPCR SYBR Green Master Mix (YEASEN). GAPDH was used as internal control.

2.15. RNA pull-down assay

The RNA-Protein Pull-Down Kit (Thermo Fisher, USA) was used to conduct the test in accordance with the manufacturer's instructions. 3 µg pure biotinylated transcripts (full length of lncHAR1B) were added to 1 mg cell lysates isolated from HUVECs and incubated for 1 h at 4 °C with rotation. The RNA-protein complex was precipitated by mixing cell protein lysate with streptavidin agarose beads. To recover proteins for use in western blotting, the beads were boiled in sodium dodecyl sulfate (SDS) buffer after being washed three times.

2.16. RNA immunoprecipitation (RIP)

Cells in a 10 cm culture dish were washed twice with ice-cold PBS and scraped off in 1 mL PBS. After centrifugation, the pellet was diluted with full RIP lysis buffer to the same volume as the original cell suspension. Overnight at 4 °C with rotation, 5 µg antibody was treated with 100 µl cell lysates in immunoprecipitation buffer. After incubating the beads with 400 µl elution buffer for 2 h, the RNA was eluted. Ethanol

was used to precipitate the eluted RNA, and RNase-free water was used to dissolve it. qRT-PCR analysis was used to identify enriched fragments.

2.17. Macrophage polarization assay

Bone marrow cells were isolated from mice femurs and tibias and were cultured for overnight. Then, nonadherent cells were cultured in α -MEM medium (Gibco) containing 10 % FBS and 30 ng/ml M-CSF. Five days later, attached cells were identified as macrophages and were treated accordingly. After 24 h, quantitative real-time polymerase chain reaction (qRT-PCR) and flow cytometry were performed.

2.18. Angiogenesis assay

In 96-well plates covered with matrigel, approximately 2×10^4 HUVECs were seeded and then incubated with corresponding treatment for 8 h. Then, a microscope was used to take pictures of the areas of interest after Calcein-AM staining. Total branch points were quantified using ImageJ software.

2.19. Transwell migration assay

Cell migration was assayed by Transwell chambers (Corning, NY, USA) experiment. In short, 200 μ L (approximately 2×10^4 HUVECs) of culture medium was added into the upper chamber, and culture medium with different treatment was put into basement chamber for 24 h, non-migratory cells in upper chamber were removed with cotton swabs, and then migratory cells were fixed in 4 % paraformaldehyde (PFA), then stained with crystal violet (0.1 %). Finally, cells were imaged with microscope and the number of migrating cells in three random fields of each sample was counted.

2.20. Diabetic mouse wound model and treatment

All experimental protocols were approved by the Institution Animal Care and Use Committee of the Tongji Medical College, Huazhong University of Science and Technology. Streptozotocin (STZ; Solarbio) was used to induce diabetes. In Brief, 10-week-old male C57/6J mice were administered with 60 mg/kg of STZ dissolved in 0.1 M phosphate-citrate buffer intraperitoneally. Mice had blood drawn from their tail veins so that glucose levels could be evaluated. When blood glucose levels were >16.7 mmol/L, an indication of diabetes, skin lesions were produced. The dorsal fur was shaved off after administering 10 ml/kg of 1 % pentobarbital sodium intraperitoneally to induce anaesthesia. The locations of the defects were indicated with a pen, and then standard, full-thickness skin wounds (diameter = 1.0 cm) were created. Mice were subsequently divided into four groups at random: control group (treated with PBS-loaded HGM-QCS hydrogels, control), diabetic group (treated with 100 μ L PBS-loaded HGM-QCS hydrogels, DM), diabetic + normoxia exosomes groups (treated with 100 μ L/100 μ L normoxic exosomes-loaded HGM-QCS hydrogels, Gel-N-Exos), and diabetic + hypoxic exosomes group (treated with 100 μ L/100 μ L hypoxic exosomes-loaded HGM-QCS hydrogels, Gel-H-Exos). The wounds were examined after the hydrogel dressings were removed on days 0, 3, 7, 10, and 14.

2.21. Histological analysis

The skin of the wound tissue was harvested on postoperative days 7 and 14, fixed with 4 % paraformaldehyde, and embedded in paraffin after dehydration. The paraffin-embedded tissues were sliced into 4- μ m-thick sections. The scar widths and the degree of collagen maturation were observed by hematoxylin and eosin (H&E) or Masson's trichrome staining. Images were examined under an optical microscope (Olympus, Japan).

2.22. Statistical analyses

GraphPad Prism 8.0 software was used for all statistical calculations. The difference between two or multiple groups was compared with Student's *t*-test or one-way ANOVA test. The results are shown as the mean \pm SD of at least three replicates of each experiment. Statistical significance was defined as a two-tailed *p* value of less than 0.05.

3. Results

3.1. Preparation and identification of exosomes

To ascertain whether hypoxic pretreatment is associated with a beneficial effect on diabetic wound healing, we collected cell culture supernatant from cells preconditioned under hypoxic conditions for 24 h. This supernatant was then added to the lower chamber of a transwell system (Fig. 1a). First, the expression level of hypoxia-inducible factor 1 alpha (HIF-1 α) was obviously upregulated in hypoxic cells after hypoxia stimulation (Fig. 1b). And then our transwell results showed that the supernatant from hypoxic preconditioned cells significantly mitigated the high glucose-induced inhibition of cell migration, showing a more positive effect than the normoxic supernatant (Fig. 1c and d). We suspected that exosomes could be the superior components in the supernatant, and hence, they were then isolated and identified. As revealed by Transmission electron microscopy (TEM), the ultrastructure displayed vesicular structured exosomes with characteristic cup-shaped morphology (Fig. 1e). And size distribution analyses further confirmed that exosomes ranged from 50 to 120 nm (Fig. 1f). The purity of exosomes was also validated through the expression of exosome-specific markers: CD9, CD63, and CD81 (Fig. 1g and h). To determine the optimal exosomes dose for further experiments, the cell viability was measured in the presence of the indicated concentrations of exosomes, which suggested that the optimal dosage of exosomes might be 100 μ g/ml in HUVECs (Fig. 1i). Additionally, we examined the uptake of PKH26-labelled exosomes in HUVECs and observed that hypoxic exosomes were taken up more efficiently than normoxic exosomes (Fig. 1j).

3.2. Hypoxic exosomes alleviate high glucose-induced dysfunctions of endothelial cells

To elucidate the effects of hypoxic exosomes in HUVECs proliferation, migration, and tube formation, we cultured HUVECs under high glucose conditions. We first analyzed HUVEC proliferation and observed a significant decrease in EdU positive nuclei when treated with high glucose conditions, an effect that was slightly reversed by normoxic exosomes (Fig. 2a and b). Intriguingly, the count of EdU positive nuclei under high glucose conditions markedly increased when pretreated with hypoxic exosomes (Fig. 2a and b). Furthermore, western blotting results indicated that high glucose treatment decreased CyclinD1 and CyclinD3 protein expression in HUVECs. The high glucose-induced inhibition of CyclinD1 and CyclinD3 expression level was partially counteracted by hypoxic exosomes (Fig. 2c). We performed scratch assays with HUVECs to assess the *in vitro* wound closure effects of exosomes. By 36 h, wound closure initiated in both the control and hypoxic exosomes groups, and the most substantial extent of wound closure was observed in the presence of hypoxic exosomes under high glucose conditions (Fig. 2d and e). Next, a transwell assay was performed to further verify the effect of hypoxic exosomes on cell migration. As depicted in Fig. 2f and g, hypoxic exosomes significantly promoted cell migration after a 24-h exposure. Moreover, the tube formation assay results showed improved tubular structures, increased numbers of tube formation, and extended tube length in the hypoxic exosomes group under high glucose conditions compared to both high glucose group and normoxic exosomes group (Fig. 2h and i). Additionally, DCF-DA staining indicated that high glucose-induced reactive oxidative stress (ROS) generation in HUVECs was significantly reduced upon treatment with hypoxic exosomes

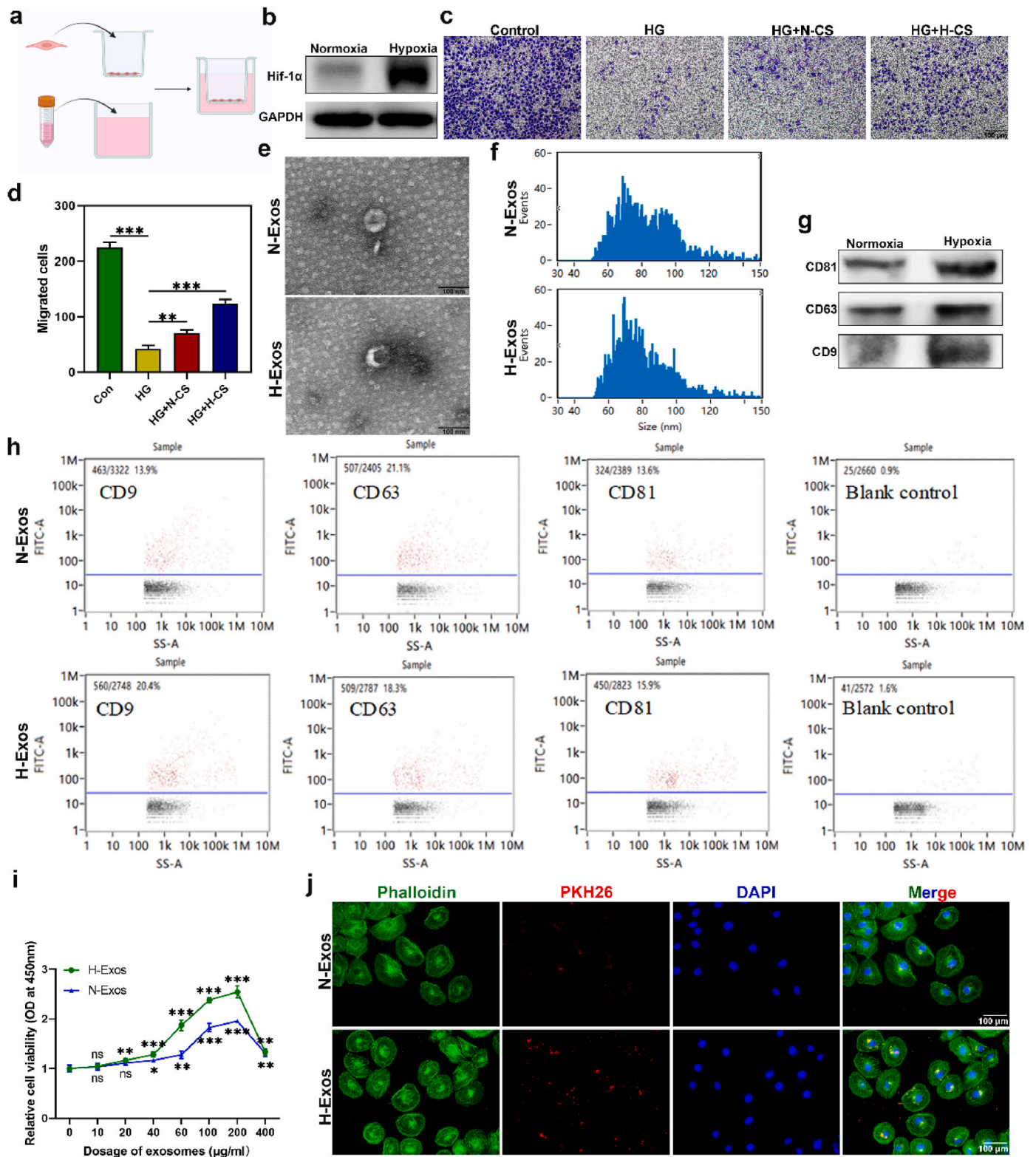


Fig. 1. Preparation and identification of exosomes. a) Schematic illustration of study design. b) Representative Western blot for HIF-1 α . c) Transwell cell migration assay. HG, high glucose condition. N-CS, cell supernatant from HUVECs *in vitro* normoxic condition. H-CS, cell supernatant from HUVECs *in vitro* hypoxic condition. d) Quantification of transwell invasion assays in (c). (e) Representative transmission electron microscope images for exosomes. f) Particle size distributions of exosomes measured by dynamic light scattering. g) Western blot analysis of exosomes markers. h) Flow cytometric analysis of exosomes markers. i) Cell viability was determined by CCK-8 assays in the presence of the indicated concentrations of exosomes. j) Labelled-normoxic and hypoxic exosomes were uptake by HUVECs (red fluorescent protein-labelled). All results are displayed as means \pm SD (n \geq 3)(*p < 0.05; **p < 0.01; ***p < 0.001).

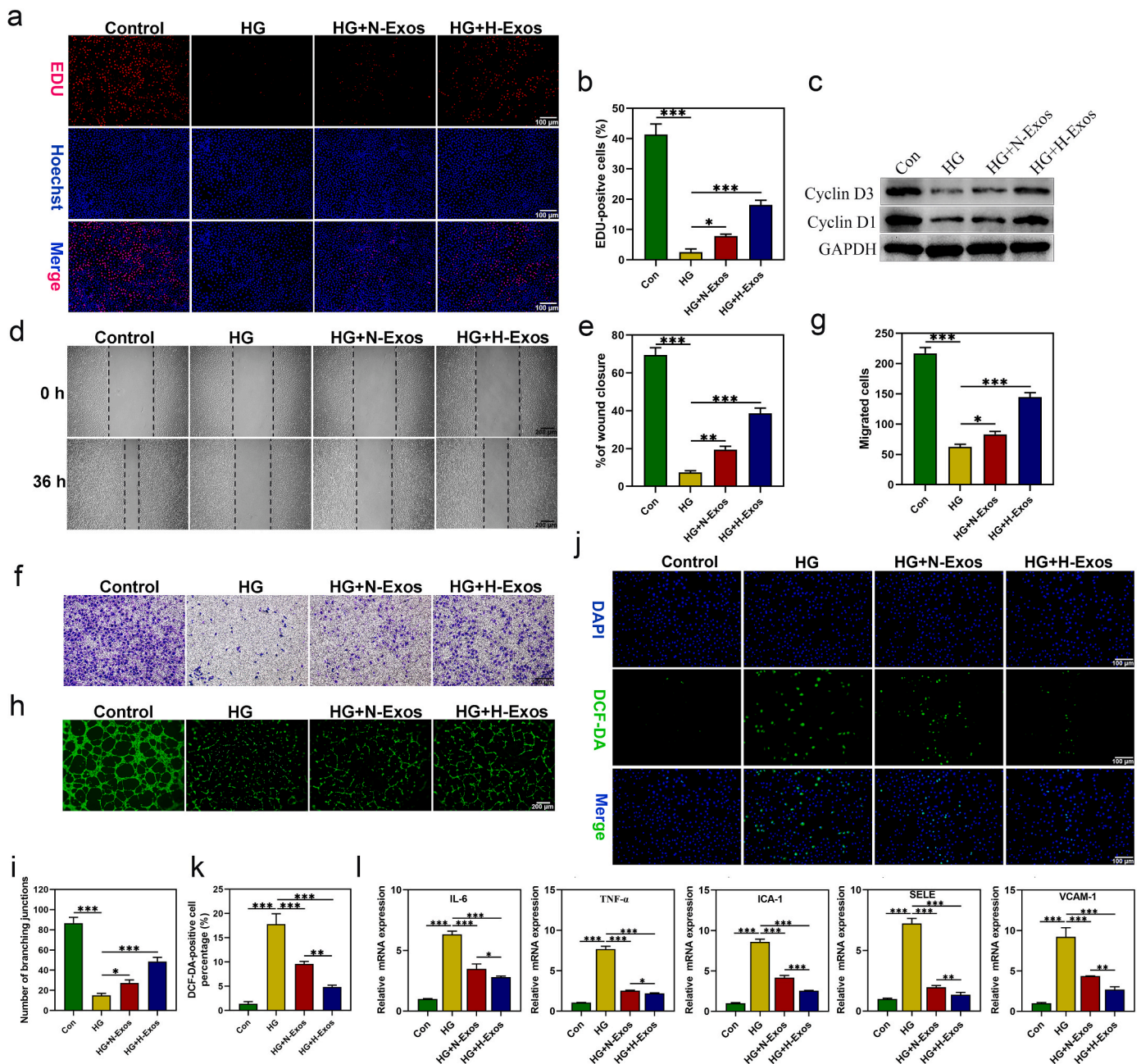


Fig. 2. Hypoxic exosomes alleviate high glucose-induced disfunctions of endothelial cells. a, b) Representative images and quantification data of immunofluorescence staining for EdU. c) Western blot analysis of CyclinD1 and CyclinD3 protein levels. d, e) Scratch assay of HUVECs and quantitative analysis. f, g) Representative images and quantification of Transwell migration for HUVECs. h, i) Representative images and relative quantification of tube pots numbers of a matrigel tube formation assay. j, k) DCF-DA staining for detecting the production of intracellular ROS (j) and quantitative analysis (k). l) qRT-PCR analysis for IL-6, TNF- α , ICA-1, SELE, VCAM-1. All results are displayed as means \pm SD (n \geq 3)(*p < 0.05; **p < 0.01; ***p < 0.001).

(Fig. 2j and k). Concurrently, hypoxic exosomes treatment resulted in decreased expression of inflammatory factors, including interleukin 6 (IL-6), tumor necrosis factor α (TNF- α), intercellular adhesion molecule 1 (ICAM-1), E-selectin (SELE), and vascular cell adhesion molecule 1 (VCAM-1) (Fig. 2l). In conclusion, hypoxic exosomes counteracted the deleterious effects of high glucose, including the inhibition of cell proliferation, migration, ROS generation, and the production of inflammatory factors.

3.3. LncCHAR1B expression is upregulated in hypoxic exosomes

To uncover the key lncRNA playing a beneficial role under high glucose conditions, we cultured cells in a hypoxic incubator chamber

with 1 % oxygen, subsequently collecting the exosomes in cell culture supernatant (Fig. 3a). Then, a comparative analysis of their respective lncRNAs expression profiles was performed. As depicted in Fig. 3b, the results demonstrated a total of 158 differentially expressed lncRNAs ($\log_2FC \geq 2$ or $\log_2FC \leq -2$, and $P < 0.01$), including 64 upregulated lncRNAs and 94 downregulated lncRNAs. Notably, lncCHAR1B, one of the most prominently upregulated lncRNAs in hypoxic exosomes, was chosen for further investigation (Fig. 3b and c). lncCHAR1B is located on chromosome 20, boasting a full length of 201930 nt. Moreover, the expression of lncCHAR1B in hypoxic exosomes and hypoxic cells was found to be significantly higher compared to that in normoxic exosomes and cells (Fig. 3d and e). Taken together, these findings suggest that lncCHAR1B is upregulated in hypoxic exosomes.

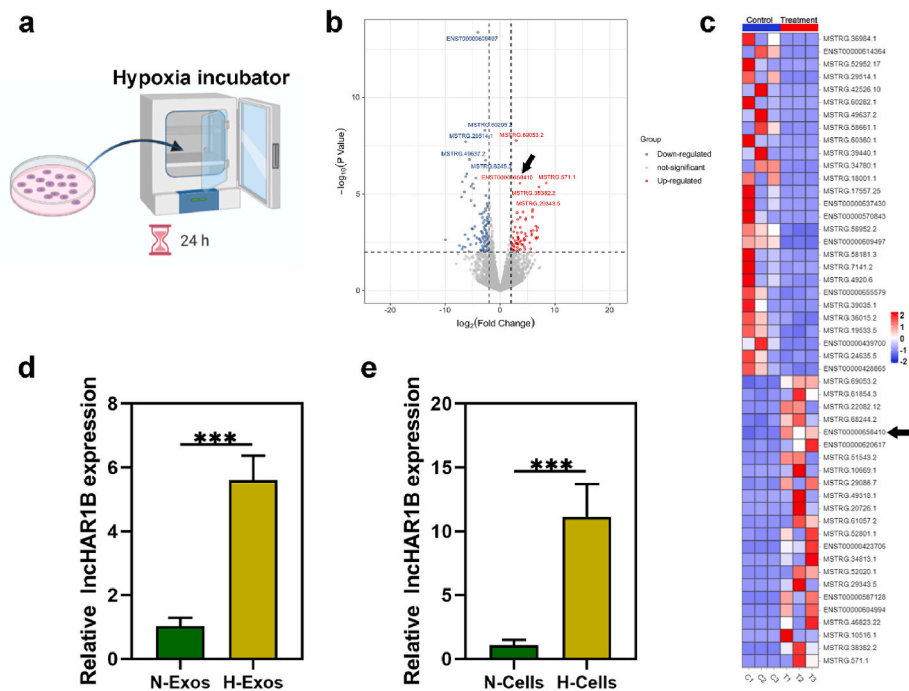


Fig. 3. LncCHAR1B expression is upregulated in hypoxic exosomes. a) The schematic diagram of treating HUVECs. b) Volcano plot of differentially expressed lncRNAs between normoxic and hypoxic exosomes. c) Heatmap of the top 50 lncRNAs. d) qRT-PCR analysis for lncCHAR1B in exosomes. e) qRT-PCR analysis for lncCHAR1B in normoxic and hypoxic HUVECs (***p* < 0.001). All results are displayed as means \pm SD (*n* \geq 3)(**p* < 0.05; ***p* < 0.01; ****p* < 0.001).

3.4. LncCHAR1B promotes cell migration and tube formation under high glucose conditions

To investigate the effects of lncCHAR1B in HUVECs under high glucose conditions, we executed lncCHAR1B overexpression in HUVECs and validated the overexpression efficiency via qRT-PCR analysis (Fig. 4a). An *in vitro* wound healing experiment demonstrated that overexpression of lncCHAR1B expedited the growth of scratch area in HUVECs under high glucose conditions, most notably in the hypoxic exosomes group (Fig. 4b and c). A transwell assay revealed that the migratory abilities of HUVECs were dampened by high glucose, but the overexpression of lncCHAR1B enhanced HUVECs' migratory capabilities under high glucose conditions, bolstering the effects of hypoxic exosomes (Fig. 4d and e). Furthermore, to assess how lncCHAR1B influences HUVECs' capacity for tube formation *in vitro*, a tube formation assay was conducted. The results indicated that high glucose drastically diminished the tube formation ability of HUVECs (Fig. 4f and g), consistent with the findings from the migration assays. However, overexpression of lncCHAR1B or/and hypoxic exosomes alleviated the inhibitory effect of high glucose in tube formation, notably increasing the number of formed tubes (Fig. 4f and g).

Collectively, these results suggest that overexpression of lncCHAR1B could counter the detrimental effects induced by high glucose and enhance cell migration and tube formation. Conversely, silencing of lncCHAR1B combined with high glucose exposure exacerbated the impairment of cell function, markedly inhibiting cell migration and tube formation (Fig. 5a–g). To further demonstrate the key role of lncCHAR1B in hypoxic exosomes, the exosomes derived by HUVECs knocked down for lncCHAR1B were harvested to study their effects. As shown in Fig. 5h–m, hypoxic exosomes from lncCHAR1B-silenced HUVECs markedly attenuated the protective effect of hypoxic exosomes in cell migration, invasion and microtubule formation under high glucose condition. Together, the results suggested lncCHAR1B might be an essential molecule in hypoxic exosomes for the protection of endothelial cell function.

3.5. LncCHAR1B promotes macrophage M2 polarization and mitigates inflammation

Given that macrophage activation and polarization play a crucial role in inflammation [31], we performed a specific experiment to investigate whether macrophage M2 polarization could be influenced by hypoxic exosomes. The macrophages were incubated with lipopolysaccharides (LPS) in the presence of stimulation with PBS or normoxic exosomes or hypoxic exosomes. After 24 h, the polarization of macrophages was analyzed by flow cytometry. The results indicated that hypoxic exosomes promoted macrophage M2 polarization (Fig. 6a and b). Then, we examined the expression of the M2 polarity markers CD206, Arginase 1 (Arg-1), CD163, and Interleukin-10 (IL-10) by qRT-PCR analysis. The mRNA levels of CD206, Arg-1, CD163, and IL-10 increased after treatment with either normoxic or hypoxic exosomes (Fig. 6c). To determine whether lncCHAR1B contributes to M2 polarization, we assessed the effect of overexpressing or silencing lncCHAR1B in macrophage polarization. We found that overexpression of lncCHAR1B increased the expression of CD206, Arg-1, CD163, and IL-10 in the presence of LPS, while silencing lncCHAR1B showed the opposite effect (Fig. 6d and e). These findings demonstrate that hypoxic HUVECs-derived exosomes induce macrophage M2 polarization, in which lncCHAR1B appears to play a pivotal role.

3.6. LncCHAR1B regulates KLF4 expression by binding to transcription factor BHLHE23

The RIsSearch software (version 2.0) predicted BHLHE23 as a potential target for lncCHAR1B. And then RNA pull-down and RIP assays confirmed the binding of lncCHAR1B to a transcription factor BHLHE23 (Fig. 7a and b). Several studies have suggested that the KLF4 gene is associated with macrophage polarization, inflammation, and diabetic wound healing [32,33]. Therefore, we explored whether lncCHAR1B could bind to the transcription factor BHLHE23 to modulate KLF4 expression. Using the JASPAR website, we predicted three potential BHLHE23 binding sites in the KLF4 promoter (Fig. 7c). We then utilized

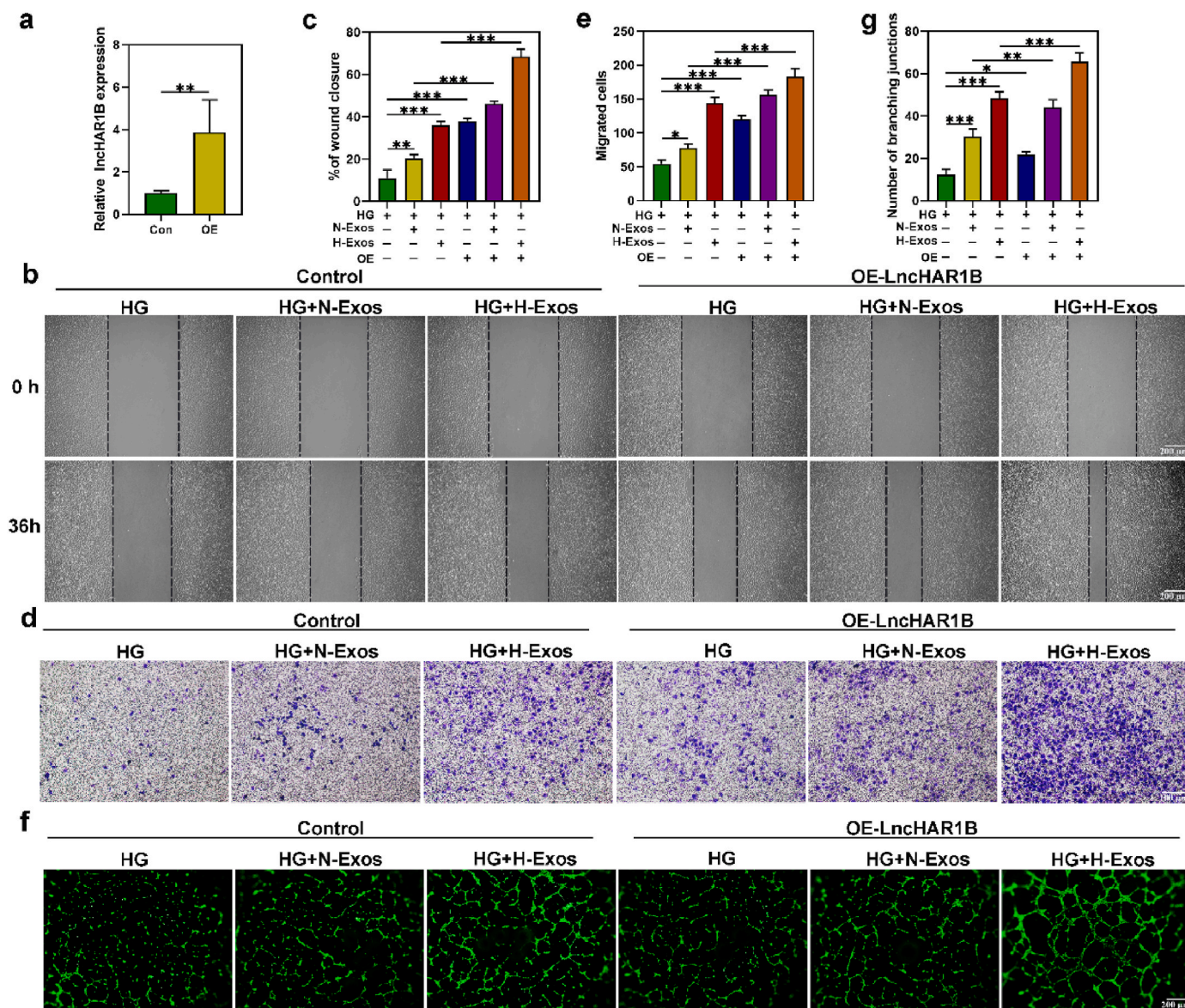


Fig. 4. IncHAR1B overexpression promotes cell migration and tube formation under high glucose conditions. a) IncHAR1B was detected by qRT-PCR assay in HUVECs after lentivirus infection. b) The migration of HUVECs transfected with the indicated lentiviral in scratch experiments. c) Quantification of the scratch wound results in (b). d) Transwell assay of HUVECs transfected with indicated lentivirus. e) Quantification of transwell migration assay in (d). f, g) Representative images and quantification analysis of tube formation assay. All results are displayed as means ± SD (n ≥ 3)(*p < 0.05; **p < 0.01; ***p < 0.001).

western blotting to assess the expression of BHLHE23 and KLF4 in HUVECs under high glucose conditions. The results showed that the addition of exosomes, especially hypoxic exosomes, led to an increase in both BHLHE23 and KLF4 expression (Fig. 7d and e). Interestingly, overexpression of IncHAR1B also led to an upregulation of BHLHE23 expression and increased KLF4 protein levels (Fig. 7f and g). Conversely, silencing of IncHAR1B not only reduced BHLHE23 levels but also decreased KLF4 expression (Fig. 7h and i). Thus, these data suggest a high degree of consistency in protein level changes between BHLHE23 and KLF4.

To delve deeper into the role of KLF4 in the protective effects mediated by hypoxic exosomes in HUVECs, we performed KLF4 silencing (Fig. 8a). Our scratch wound healing assay, migration, and tube formation experiments showed that KLF4 silencing significantly worsened the high glucose-induced endothelial impairment. Moreover, it noticeably antagonized the protective effect of hypoxic exosomes (Fig. 8b–g). Taken together, these results strongly suggest that IncHAR1B might bind to the transcription factor BHLHE23 to regulate

KLF4 expression.

3.7. Characterization of HGM-QCS hydrogels

Scanning Electron Microscopy (SEM) images of HGM-QCS hydrogels depicted their characteristic 3D porous topologies (Fig. 9a). Similar porous structures were observed in samples with 0 %, 1 %, 2 % and 3 % QCS hydrogels, although their pore sizes varied. The HGM-QCS hydrogels with less than 2 % QCS displayed more micropores compared to the 3 % QCS hydrogel, and the pore sizes were much larger than that of exosomes, which provided a structural basis for loading exosomes into the HGM-QCS hydrogels (Fig. 9b). SEM results corroborated that 1 % and 2 % QCS hydrogel samples swelled less than the 3 % QCS sample, suggesting that the network structure of the 1 % and 2 % QCS samples is more robust and stable (Fig. 9c). A concentration of QCS higher than 3 % resulted in a substantial increase in the Young’s modulus of HGM-QCS hydrogels, almost doubling compared to the 1 % and 2 % QCS hydrogels (Fig. 9d). Moreover, time-sweep experiments were conducted to

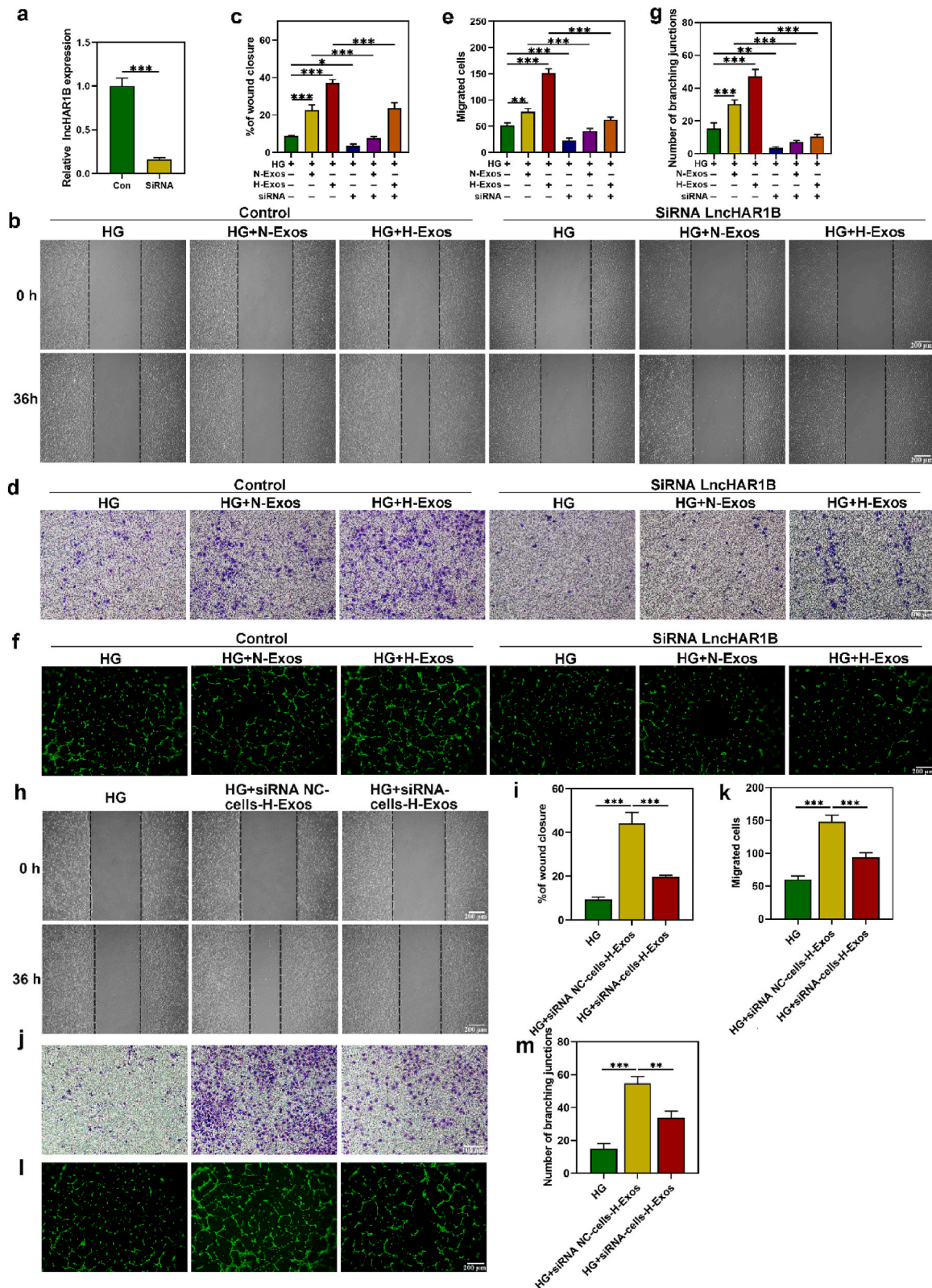


Fig. 5. LncHAR1B silencing antagonizes the beneficial effect of hypoxic exosomes in HUVECs under high glucose conditions. a) LncHAR1B was detected by qRT-PCR assay in HUVECs after siRNA infection. b, c) The migration of HUVECs transfected with the indicated siRNA in scratch experiments. c) Quantification of the scratch wound results in (b). d, e) Representative images and quantification analysis of transwell migration assay. f, g) Representative images and quantification analysis of tube formation assay. h-m) Exosomes secreted by cells knocked down for LncHAR1B were collected, and were used to the further experiments. Representative scratch assays (h) and its corresponding quantification (i). j-m) Representative images and quantification of the transwell migration and tube formation assays. All results are displayed as means ± SD (n ≥ 3) (*p < 0.05; **p < 0.01; ***p < 0.001).

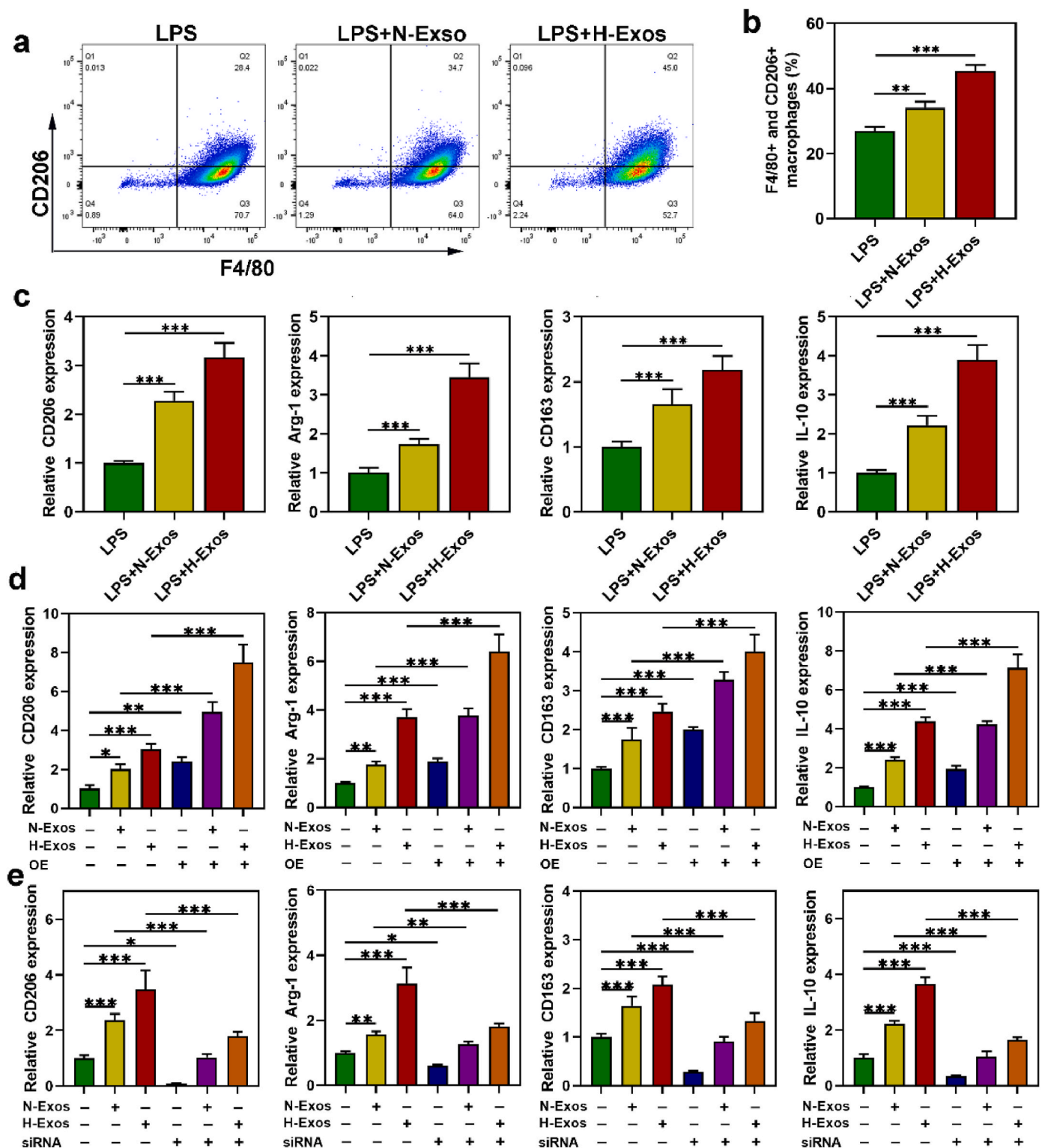


Fig. 6. LncHAR1B promotes macrophage M2 polarization and mitigates inflammation. a) Flow cytometry was used to explore the macrophage M2 polarization. b) The quantification analysis of the results in (a). c) qRT-PCR assay for CD206, Arg-1, CD163 and IL-10 was carried out after corresponding treatment. d) qRT-PCR analysis for CD206, Arg-1, CD163 and IL-10 in macrophages transfected with the indicated lentivirus. e) qRT-PCR analysis for CD206, Arg-1, CD163 and IL-10 in macrophages transfected with the indicated siRNA. All results are displayed as means \pm SD ($n \geq 3$) (* $p < 0.05$; ** $p < 0.01$; *** $p < 0.001$).

monitor changes in the storage modulus (G') and loss modulus (G'') of HGM-QCS hydrogels with different QCS concentrations under UV irradiation (Fig. 9e). All samples demonstrated an instantaneous and uniform increase in the elastic modulus, which remained constant after 180 s (Fig. 9e). *In vitro* experiments revealed that HGM-QCS hydrogels

underwent gradual degradation at a relatively slow rate, with approximately 50 % of the HGM-QCS hydrogel degraded by 14 days (Fig. 9f). The release of exosomes from mixed HGM-QCS hydrogels with 2% QCS (Gel-Exos) was assessed *in vitro* (Fig. 9g). Initial release occurred at a relatively high rate, slowing down in a later phase. Over 60 % of

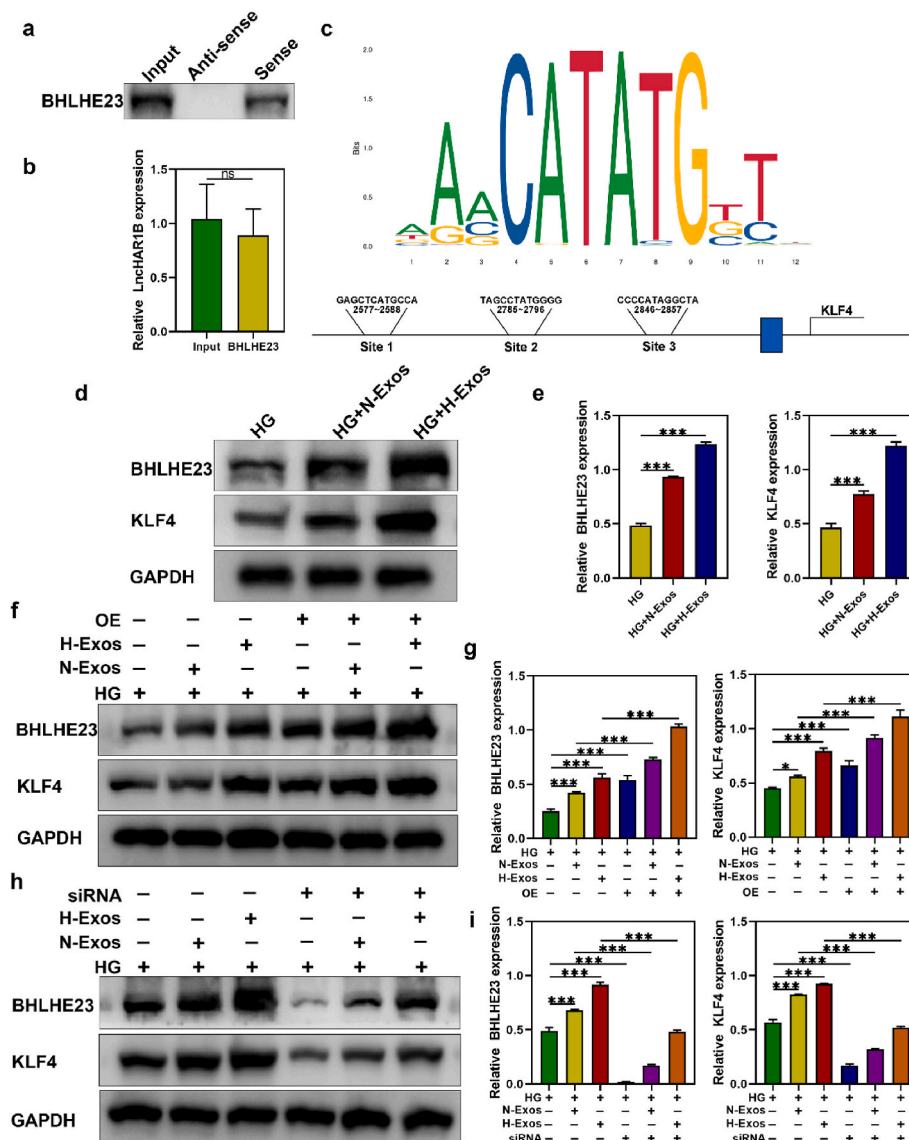


Fig. 7. LncCHAR1B regulates KLF4 expression by binding to transcription factor BHLHE23. **a)** RNA-pull down assay verified physical interaction between LncCHAR1B and BHLHE23. **b)** RIP assay was used to determine the level of LncCHAR1B. **c)** The potential binding sites between BHLHE23 and KLF4 were inspected by JASPAR website. **d)** The proteins expression of BHLHE23 and KLF4 was determined by Western blot assay upon high glucose, high glucose (HG) + normoxic exosomes (N-Exos) and HG + hypoxic exosomes (H-Exos) stimulation. **e)** Quantitative analysis of Western blot in (d). **f, g)** Representative western blotting and quantitative analysis of BHLHE23 and KLF4 proteins expression in HUVECs after transfection with the indicated lentivirus. **h)** Representative Western blot images and quantitative analysis in HUVECs after transfection with indicated siRNA. All results are displayed as means \pm SD ($n \geq 3$) (* $p < 0.05$; ** $p < 0.01$; *** $p < 0.001$).

exosomes were released within the first 12 h, while release over the remaining 60 h was significantly slower. Therefore, exosome release from the mixed hydrogels continued for over 72 h (Fig. 9g).

It is known that QCS has significant antibacterial properties against *Escherichia coli* (*E. coli*), *Staphylococcus aureus* (*S. aureus*), etc [34,35]. Consequently, we evaluated the antimicrobial activity of the HGM-QCS hydrogel with 2% QCS coating PBS (Control or Gel) or exosomes (Gel-Exos), and observed clear antibacterial activity against *E. coli*, *S. aureus* and MRSA in the HGM-QCS hydrogel, and exosomes loading did not affect the antibacterial activity of the hydrogel (Fig. 9h and i). Therefore, HGM-QCS hydrogels with 2% QCS was chosen to deliver exosomes based on above data.

Subsequently, we used live/dead cell staining assays with HUVECs and mouse embryonic fibroblast (NIH3T3) to assess the cellular compatibility of the Gel-Exos samples. Active cells (stained with calcein-AM) emitted green fluorescence, whereas dead cells (stained with PI) emitted red fluorescence. After 3 days, HUVECs or NIH3T3 adhered to

the hydrogels, and all samples demonstrated good cytocompatibility, with only a negligible number of dead cells visible (Fig. 9j and k). Further, to assess the *in vivo* side effects of the hydrogels, various organs were harvested. No histological differences in the heart, liver, spleen, lung and kidney were observed in the Gel-Exos groups by H&E staining, indicating that there was no notable toxicity (Fig. 9l). These results collectively demonstrated that Gel-Exos exhibit excellent properties such as antibacterial activity, outstanding biocompatibility, and sustained exosome release.

3.8. Gel-Exos accelerates diabetic wound healing

Subsequently, we investigated whether the hypoxic exosomes can speed up diabetic wound healing *in vivo*. To achieve exosomes sustained release, HGM-QCS hydrogels with 2% QCS were employed in this study. Then, full-thickness wounds on the back of C57/6J mice were locally treated with PBS-loaded HGM-QCS hydrogels (Control or DM groups),

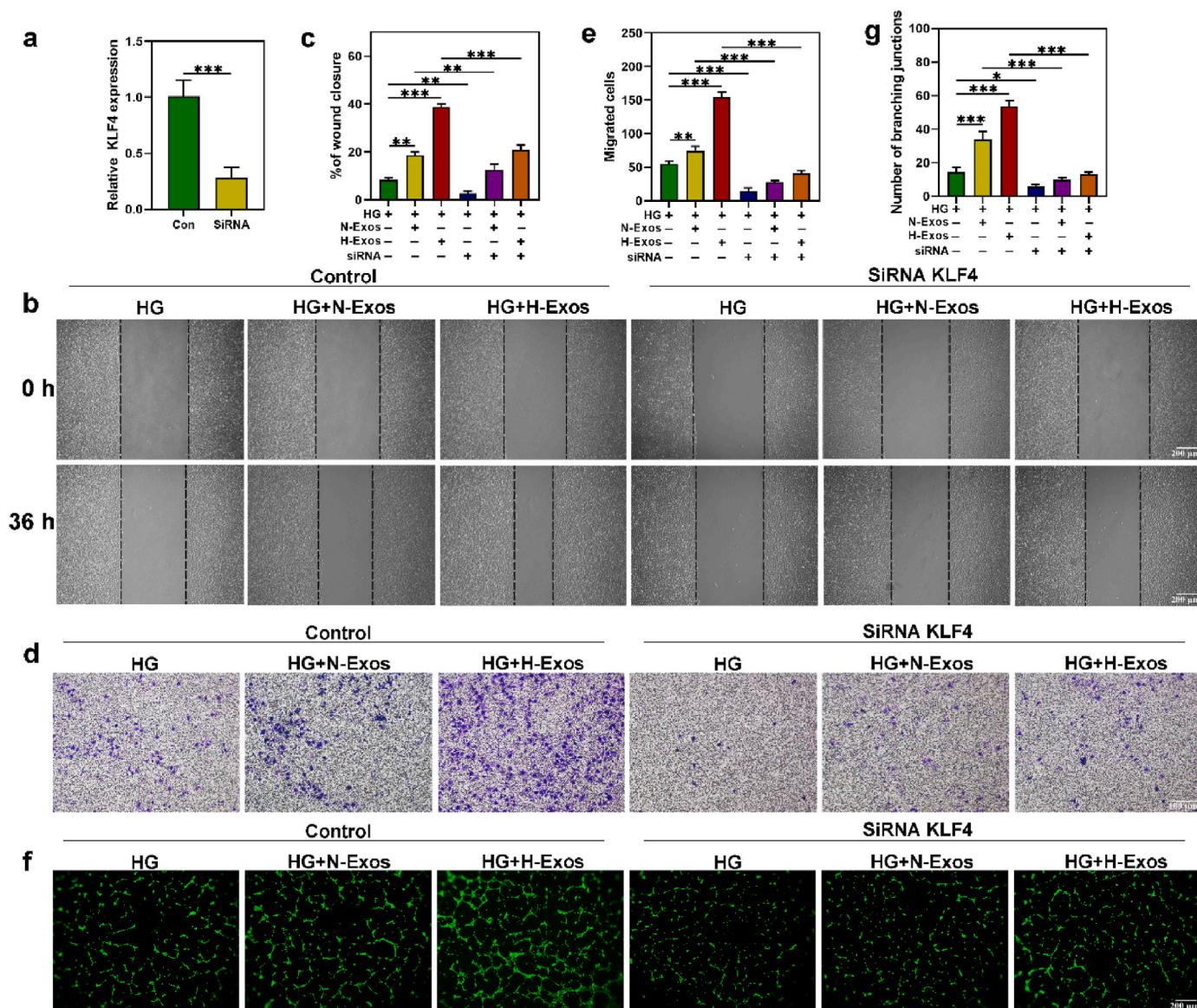


Fig. 8. KLF4 silencing exacerbates the high glucose-induced endothelial impairment. a) The effect of KLF4 silencing was validated by qRT-PCR analysis. b) Wound healing scratch experiments after infection with KLF4 siRNA. c) Quantitative analysis of the migration area of scratch wound assay. d) Transwell migration assay with the 12-well transwell system and quantitative analysis (e). f) Tube formation assay *in vitro*. g) Quantification of tube formation. All results are displayed as means \pm SD ($n \geq 3$) (* $p < 0.05$; ** $p < 0.01$; *** $p < 0.001$).

normoxic exosomes-loaded HGM-QCS hydrogels (Gel-N-Exos group) and hypoxic exosomes-loaded HGM-QCS hydrogels (Gel-H-Exos). After surgery, no animals died or showed signs of abnormalities. Wounds in control mice demonstrated quicker hemostasis, while diabetic wounds in DM group exhibited an opposite trend. Notably, local administration of Gel-Exos, particularly Gel-H-Exos, significantly expedited the wound healing process compared to the DM group, as validated by gross observations (Fig. 10a). Wound areas were measured on days 0, 3, 7, 10 and 14. Diabetic mice treated with Gel-Exos displayed faster wound closure on days 3, 7 and 14 post-wounding compared to the DM group (Fig. 10b and c). Rapid healing in the Gel-H-Exos group was observed between days 7 and 14, similar to the control group. By day 14, wounds in control group and Gel-H-Exos group were completely healed, while wounds in DM group remained approximately 50 % of their original size. Evidently, hypoxic exosomes exerted a pro-healing effect, as the degree of wound healing in this group significantly surpassed that of the normoxic exosomes groups.

After 7 and 14 days postwounding, different histological studies

were implemented to characterize the wound tissue in addition to directly monitoring the changes of wound regions. On days 7 and 14, representative H&E images of the wounds treated using the aforementioned approaches are shown in Fig. 10d. In diabetic mice, the narrowest scar widths were found in Gel-H-Exos group at days 7 and 14 post-wounding, almost reaching that of the control group, followed by Gel-N-Exos group (Fig. 10d and e). Collagen fibres were stained with Masson's trichrome to examine the impact of hypoxia exosomes on collagen deposition and remodeling. Gel-Exos groups, especially the Gel-H-Exos group, showed enhanced collagen deposition and collagen fibres were regularly oriented by day 7 (Fig. 10f and g). The Gel-N-Exos and Gel-H-Exos groups continued to show enhanced collagen deposition and typical bundle-shaped collagen fibres on days 14, whereas the DM group showed a disordered appearance with inflammatory cell infiltration.

Additionally, the expression level of BHLHE23 and KLF4 was analyzed in the wound tissues. As shown in Fig. 11a, b, f and g, increased protein levels of BHLHE23 and KLF4 were observed in Gel-Exos groups, especially Gel-H-Exos group, compared with DM group, in consistent

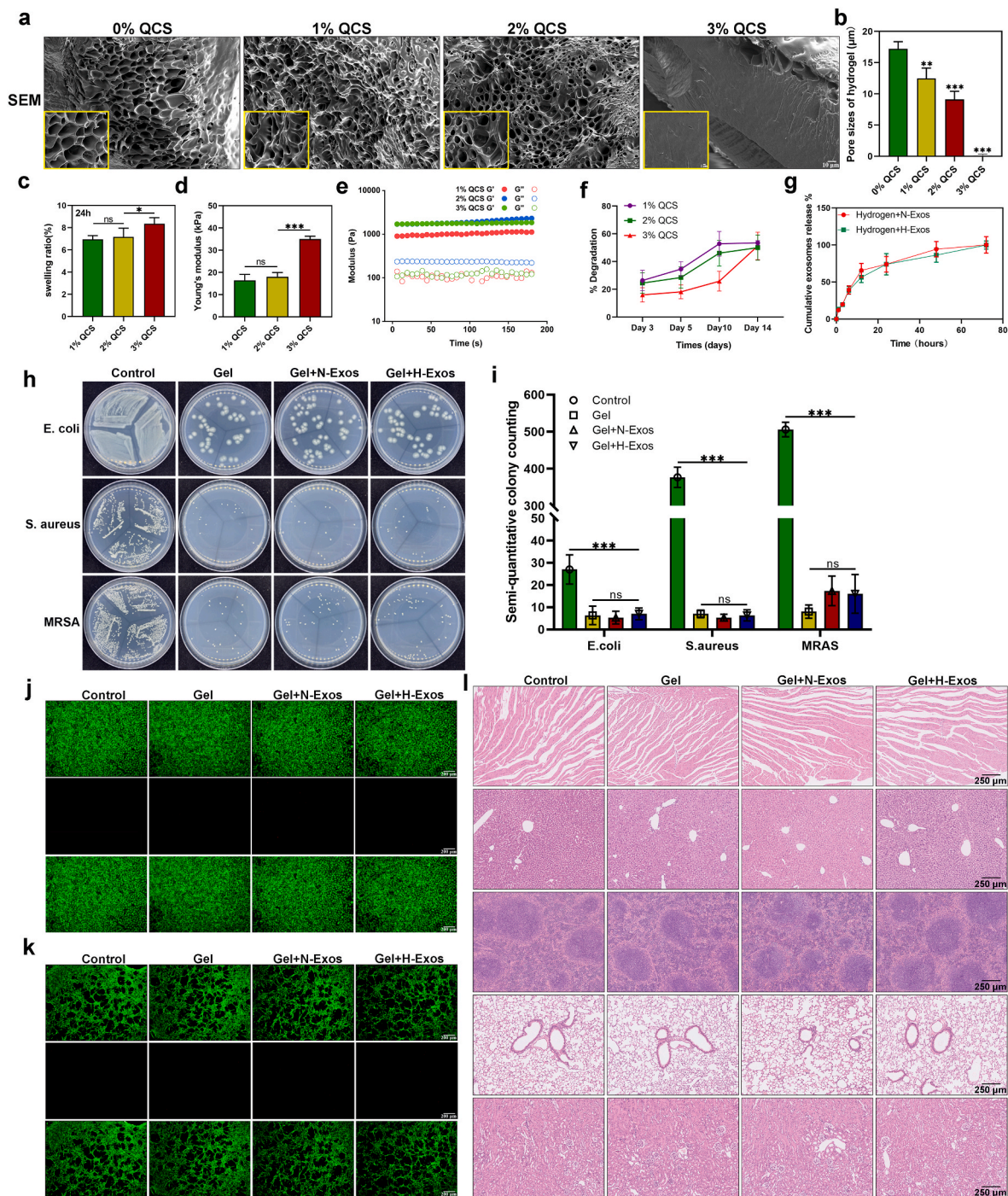


Fig. 9. Characterization of HGM-QCS hydrogels. a) SEM images of HGM-QCS hydrogels. b) The average pore size of the HGM-QCS hydrogels. c) Equilibrium swelling ratio of HGM-QCS hydrogels after swelling for 24 h in PBS (pH 7.4) at 37 °C. d) The average Young's modulus of the three hydrogels. e) Rheological analysis involving the storage modulus (G') and loss modulus (G'') under 1 mW/cm² 365 nm light irradiation. f) Degradation profiles of HGM-QCS hydrogels in PBS (pH7.4, 37 °C). g) Exosomes release curves from Gel-Exos. h) Photographs of the agar plates of *E. coli*, *S. aureus* and MRSA in HGM-QCS with PBS or exosomes. i) The corresponding bacterial counts (CFU mL⁻¹) in panel. j,k) Live/dead fluorescence of HUVECs cells (j) and the mouse embryonic fibroblast (NIH3T3) cultured in the surface layer of HGM-2% QCS hydrogels hydrogels for 3 days. l) Toxicity of HGM-QCS hydrogels was detected with H&E staining *in vivo*. All results are displayed as means \pm SD ($n \geq 3$)(* $p < 0.05$; ** $p < 0.01$; *** $p < 0.001$).

with experiments *in vitro*. Then, to explore the effects of exosomes for macrophages polarization *in vivo*, immunofluorescence for CD11b (a marker of macrophages) and Arg-1 (a marker of M2 macrophages) was performed. In addition to the control group, more macrophages were detected in the DM group, followed by Gel-N-Exos group, and the fewest macrophages were observed in Gel-H-Exos group on day 7 and 14 (Fig. 11c and h), while the number of M2 macrophage displayed the

opposite trend (Fig. 11d and i).

During wound healing, new blood vessel formation is crucial for transport of trophic factors to wound sites. We next investigated whether treatment with Gel-Exos could promote angiogenesis in wound sites, thereby enhancing diabetic wound healing. As shown in Fig. 11e and j, CD31, a marker of angiogenesis, exhibited increased expression in Gel-N-Exos and Gel-H-Exos groups, and more vessels marked with CD31

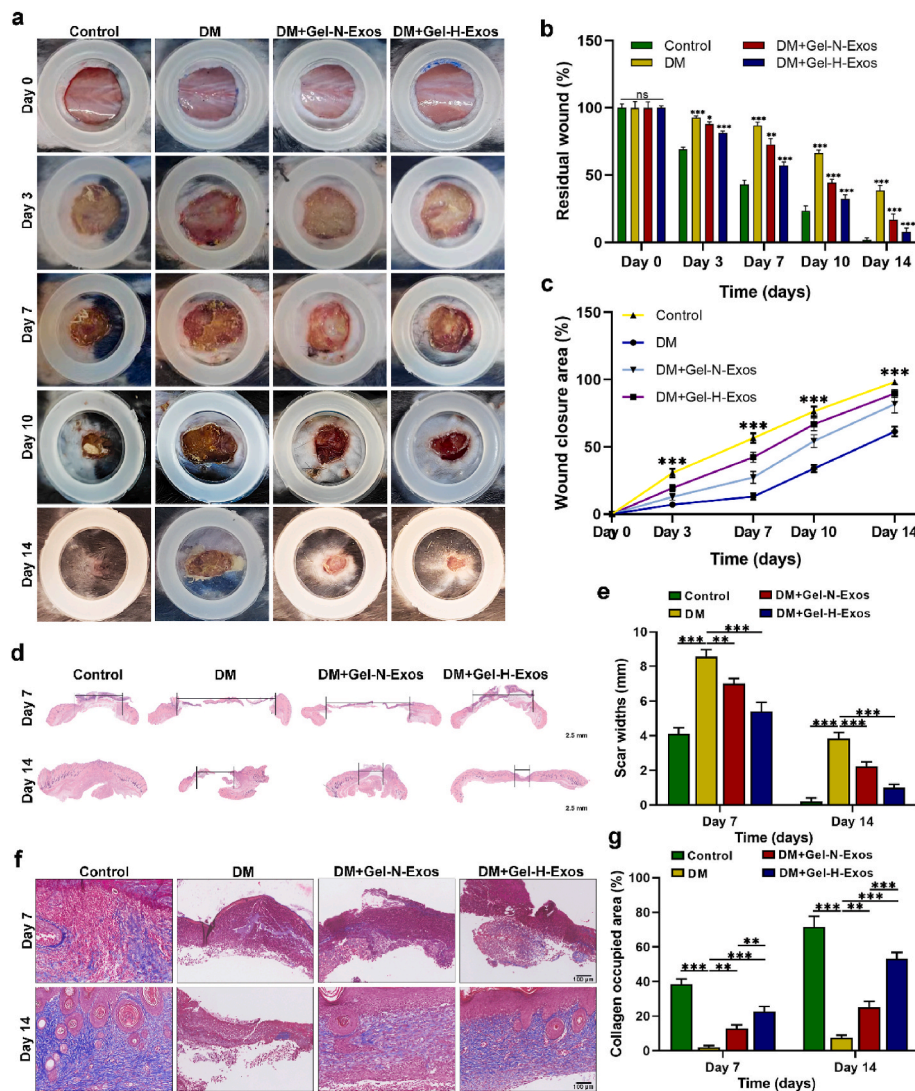


Fig. 10. Wound healing promoting effects of Gel-H-Exos hydrogels. a) Gross view of wounds at days 0, 3, 7, 10, and 14. b) Statistical analysis of the residual wound area in each group. c) Statistical analysis of wound closure area. d) Representative images of scar widths stained by H&E. e) Statistical analysis of the scar widths in each group. f) Masson's trichrome staining was used to stain collagen fibers and the collagen fiber was stained in blue. g) Statistical analysis of collagen occupied area. All results are displayed as means \pm SD ($n \geq 3$)(* $p < 0.05$; ** $p < 0.01$; *** $p < 0.001$).

were observed in Gel-H-Exos group compared with Gel-N-Exos and DM groups on day 7 and 14. Collectively, these findings suggested that diabetic wound healing was aided by Gel-H-Exos via multiple mechanisms, such as collagen deposition, M2 polarization and angiogenesis.

4. Discussion

Exosomes, being natural nanoscale vesicles, have revolutionized the field of intercellular communication by serving as vital mediators of cell-to-cell crosstalk. These extracellular vesicles are endowed with a diverse cargo of proteins, nucleic acids, lipids, and metabolites, making them highly attractive candidates for therapeutic interventions in a plethora of diseases [36]. In our study, we endeavored to unravel the enigmatic impact of hypoxic exosomes released by HUVECs on neighboring endothelial cells and macrophages under high glucose conditions. The results of our investigation not only unveiled promising improvements in cell migration, tube formation, and a reduction in excessive inflammation but also illuminated the underlying molecular mechanisms that potentially govern diabetic wound healing and tissue repair. The focal point of intrigue lies in the enrichment of lncRNAs within these hypoxic exosomes, with particular emphasis on lncHAR1B. The vast and diverse

roles of lncRNAs in regulating gene expression, chromatin remodeling, transcriptional and post-transcriptional regulation, and epigenetic modifications have recently come to the forefront of molecular biology. In the context of hypoxic exosomes, these enigmatic lncRNAs may orchestrate complex regulatory networks that influence cellular behavior and dictate the wound healing responses under high glucose conditions. To unlock the full potential of these lncRNAs, it becomes imperative to delve deeper into their functional significance, identify their target genes, and elucidate the molecular mechanisms through which they exert their influence. Such comprehensive investigations could pave the way for innovative therapeutic approaches, potentially targeting specific lncRNAs to enhance diabetic wound healing and promote tissue regeneration.

For the treatment of diabetic wounds, various biomaterials have recently been employed to enhance the retention period of exosomes and control the release of therapeutic molecules *in vivo* [37]. The efficiency of loading healing chemicals into exosomes, and subsequently into biomaterials, is a critical factor determining the success of this treatment approach. In this investigation, we devised a methodology to successfully prepare exosomes-loaded HGM-QCS hydrogels (Gel-Exos), characterized by their antibacterial activity, exceptional

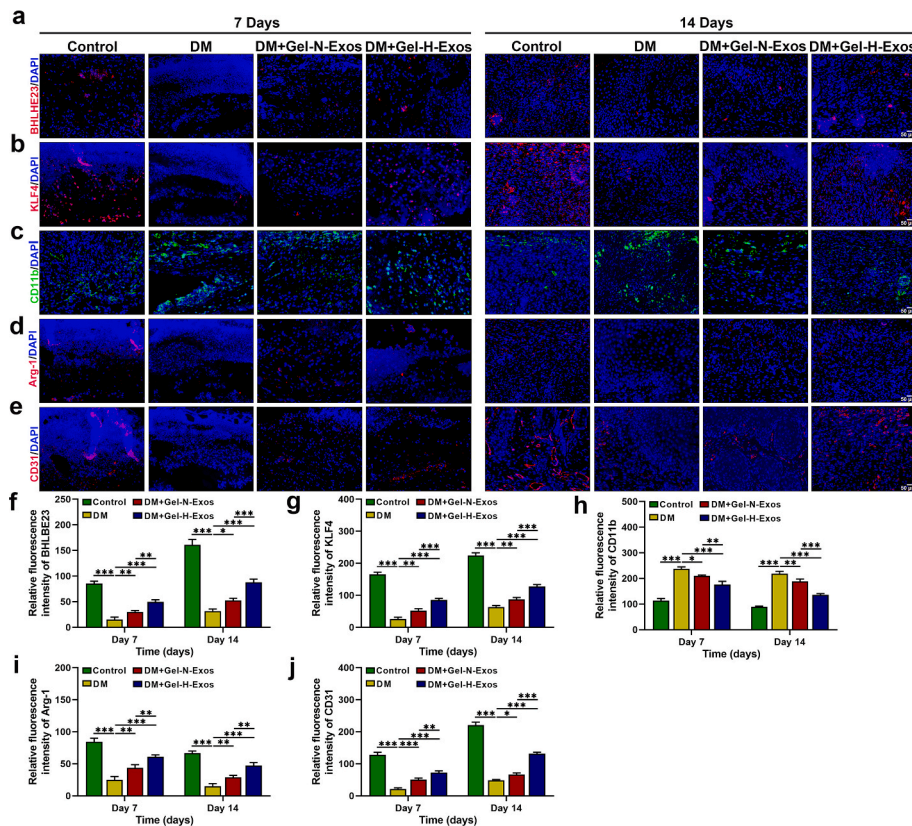


Fig. 11. The Gel-H-Exos promote macrophages M2 polarization and increase neovascularization of diabetic wounds. a–e) Immunofluorescence of BHLHE23, KLF4, CD11b, Arg-1 and CD31 of the wound tissue. f–j) Statistical analyses of BHLHE23, KLF4, CD11b, Arg-1 and CD31 immunofluorescence. All results are displayed as means ± SD (n ≥ 3)(*p < 0.05; **p < 0.01; ***p < 0.001).

biocompatibility, and sustained exosomes release. Furthermore, diabetic wound healing was significantly improved via the mechanisms of collagen deposition, M2 macrophage polarization and neovascularization when using Gel-H-Exos *in vivo*. A schematic representation of Gel-H-Exos hydrogels aiding diabetic wound healing can be found in Fig. 12.

While numerous studies have reported the beneficial role of hypoxia exosomes in diabetic wound healing [15,16,38], few have explored the interactions of hypoxic HUVECs-derived exosomes within the specific context of diabetic wound healing. This represents a largely untapped research area in the field of diabetic wound treatments. Previous research has indicated that hypoxia adipose stem cell-derived exosomes

accelerated the diabetic wound healing process [15,16,38], and demonstrated significant advantages in tissue repair and regeneration [39,40], lending some degree of validation to our study results. Moreover, recent research has revealed that many lncRNAs are aberrantly expressed under hypoxia, signifying the complexity of hypoxia-responsive gene reprogramming and underlining the importance of acknowledging the involvement of non-coding genes in this adaptation. Consequently, we proceeded to investigate the role of lncRNAs within hypoxic exosomes in diabetic wound healing.

There is mounting evidence that lncRNAs attach to target proteins in order to carry out their biological roles [41]. Various mechanisms, such as influencing protein expression and activity, altering protein subcellular localization, and serving as structural components, contribute to the regulatory role of lncRNAs in their interactions with proteins [42]. Then, BHLHE23 was identified as a potential target of lncHAR1B action by RIsearch software, a finding further corroborated by RNA pull-down assays. The specific effect of BHLHE23, known to be a transcriptional regulator factor [43,44], remains unexplored in the field of diabetic wound healing. BHLHE23 was observed to be upregulated when lncHAR1B was overexpressed and downregulated when lncHAR1B was knocked out, signifying a strong positive correlation between lncHAR1B and BHLHE23. Additionally, we discovered that the expression level of KLF4 was regulated subsequent to the binding of lncHAR1B with BHLHE23, indicating that KLF4 could potentially be a target gene for the transcription factor BHLHE23 *in vitro* experiments. As already reported in the studies, KLF4 plays a pivotal role in diabetic wound healing by inhibition of inflammatory and skewing their polarization towards M2 macrophages [33,45]. In summary, our data demonstrated that lncHAR1B bound to BHLHE23, and subsequently activated KLF4 expression to perform their biological function.

Finally, to ensure the sustained release and maintained activity of

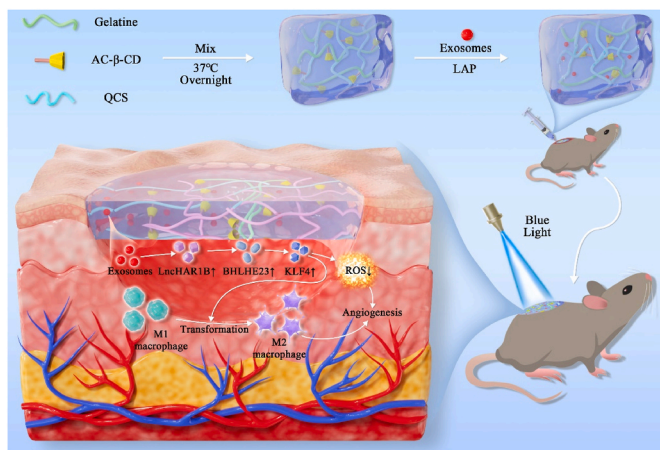


Fig. 12. Schematic representation of the Gel-H-Exos for the diabetic wound healing.

hypoxic exosomes, we introduced HCG-QCS hydrogels with 2% QCS as an encapsulating agent to create a novel wound dressing. *In vitro* experiments demonstrated superior antibacterial activity, biocompatibility, and sustained exosomes release. Meanwhile, *in vivo* experiments affirmed that Gel-H-Exos not only furnish an effective method for treating diabetic wounds by boosting angiogenesis and M2 macrophages polarization, processes accompanied by enhanced collagen deposition, but also establish a proficient exosomes delivery platform.

5. Conclusion

Taken together, our findings elucidate that hypoxia-induced lncHAR1B within exosomes protects HUVECs from the detrimental effects of high glucose, including an amplified inflammatory response and reduced migration and tube formation capabilities. Furthermore, this research provides a connection between lncHAR1B and the BHLHE23/KLF4 axis in endothelial cells and macrophages. In *in vivo* experiments, the Gel-H-Exos were shown to expedite the healing of diabetic wounds by promoting angiogenesis and M2 macrophages polarization. In essence, this study not only provides potentially innovative therapeutic strategies for accelerating diabetic wound healing, but also contributes towards the development of a practical exosome delivery platform.

Data availability

All data of this study are available within the paper.

Ethical approval and consent to participate

The Institutional Animal Care and Use Committee of the Tongji Medical College, Huazhong University of Science and Technology approved all animal studies.

CRediT authorship contribution statement

Peng Cheng: Conceptualization, Data curation, Formal analysis, Investigation, Methodology, Project administration, Software, Writing – original draft. **Xudong Xie:** Conceptualization, Data curation, Formal analysis, Investigation, Methodology, Writing – original draft. **Liangcong Hu:** Data curation, Formal analysis, Investigation, Methodology, Project administration, Resources, Writing – original draft. **Wu Zhou:** Conceptualization, Data curation, Formal analysis, Investigation, Methodology, Validation, Writing – original draft. **Bobin Mi:** Conceptualization, Data curation, Formal analysis, Investigation, Writing – original draft, Writing – review & editing. **Yuan Xiong:** Conceptualization, Data curation, Investigation, Supervision, Validation, Visualization. **Hang Xue:** Data curation, Formal analysis, Investigation, Methodology, Resources, Software, Visualization. **Kunyu Zhang:** Formal analysis, Methodology, Project administration, Software. **Yuxiao Zhang:** Data curation, Investigation, Methodology, Project administration, Software, Visualization. **Yiqiang Hu:** Data curation, Investigation, Methodology, Software, Validation. **Lang Chen:** Investigation, Methodology, Software, Validation, Visualization. **Kangkang Zha:** Conceptualization, Data curation, Investigation, Supervision, Validation, Visualization. **Bin Lv:** Data curation, Formal analysis, Methodology, Project administration, Supervision. **Ze Lin:** Data curation, Methodology, Project administration, Visualization. **Chuanlu Lin:** Resources, Software, Validation. **Guandong Dai:** Investigation, Software, Supervision, Visualization. **Yixin Hu:** Software, Supervision, Validation, Visualization. **Tengbo Yu:** Conceptualization, Formal analysis, Methodology, Writing – original draft, Writing – review & editing. **Hankun Hu:** Conceptualization, Formal analysis, Resources, Software, Writing – original draft, Writing – review & editing. **Guohui Liu:** Conceptualization, Data curation, Funding acquisition, Investigation, Methodology, Project administration, Writing – original draft, Writing – review & editing. **Yingze Zhang:** Conceptualization, Data curation,

Formal analysis, Investigation, Methodology, Resources, Software, Validation, Writing – original draft, Writing – review & editing.

Declaration of competing interest

All authors declare no competing financial interests.

Acknowledgements

This work was supported by the National Science Foundation of China (No. 82272491, No. 82072444). Chinese Pharmaceutical Association Hospital Pharmacy department (No. CPA-Z05-ZC-2022-002); Grants from Hubei Province Unveiling Science and Technology Projects (No. 2022–35).

References

- [1] G.C. Gurtner, S. Werner, Y. Barrandon, Wound repair and regeneration, *Nature* 453 (2008) 314–321.
- [2] S.A. Eming, P. Martin, M. Tomic-Canic, Wound repair and regeneration: mechanisms, signaling, and translation, *Sci. Transl. Med.* 6 (2014), 265sr266.
- [3] J. Inaishi, Y. Saisho, Beta-cell mass in obesity and type 2 diabetes, and its relation to pancreas fat: a mini-review, *Nutrients* (2020) 12.
- [4] A.J. Martí-Carvajal, C. Gluud, S. Nicola, Growth factors for treating diabetic foot ulcers, *Cochrane Database Syst. Rev.* 2015 (2015), Cd008548.
- [5] R. Nunan, K.G. Harding, P. Martin, Clinical challenges of chronic wounds: searching for an optimal animal model to recapitulate their complexity, *Dis. Model Mech.* 7 (2014) 1205–1213.
- [6] S. Ela, I. Mäger, X.O. Breakefield, Extracellular vesicles: biology and emerging therapeutic opportunities, *Nat. Rev. Drug Discov.* 12 (2013) 347–357.
- [7] M. Tkach, C. Théry, Communication by extracellular vesicles: where we are and where we need to go, *Cell* 164 (2016) 1226–1232.
- [8] S. Sjöqvist, T. Ishikawa, D. Shimura, Exosomes derived from clinical-grade oral mucosal epithelial cell sheets promote wound healing, *J. Extracell. Vesicles* 8 (2019), 1565264.
- [9] X. Kou, X. Xu, C. Chen, The Fas/Fap-1/Cav-1 complex regulates IL-1RA secretion in mesenchymal stem cells to accelerate wound healing, *Sci. Transl. Med.* 10 (2018).
- [10] H. Kim, S.Y. Wang, G. Kwak, Exosome-guided phenotypic switch of M1 to M2 macrophages for cutaneous wound healing, *Adv. Sci.* 6 (2019), 1900513.
- [11] Y. Xiong, Z. Lin, P. Bu, A whole-course-repair system based on neurogenesis-angiogenesis crosstalk and macrophage reprogramming promotes diabetic wound healing, *Adv. Mater.* (2023), e2212300.
- [12] C.Y. Chen, S.S. Rao, L. Ren, Exosomal DMBT1 from human urine-derived stem cells facilitates diabetic wound repair by promoting angiogenesis, *Theranostics* 8 (2018) 1607–1623.
- [13] L. Li, J. Mu, Y. Zhang, Stimulation by exosomes from hypoxia preconditioned human umbilical vein endothelial cells facilitates mesenchymal stem cells angiogenic function for spinal cord repair, *ACS Nano* 16 (2022) 10811–10823.
- [14] Y. Zhang, Z. Hao, P. Wang, Exosomes from human umbilical cord mesenchymal stem cells enhance fracture healing through HIF-1 α -mediated promotion of angiogenesis in a rat model of stabilized fracture, *Cell Prolif.* 52 (2019), e12570.
- [15] J. Wang, H. Wu, Y. Peng, Hypoxia adipose stem cell-derived exosomes promote high-quality healing of diabetic wound involves activation of PI3K/Akt pathways, *J. Nanobiotechnol.* 19 (2021) 202.
- [16] R. Shi, Y. Jin, S. Zhao, Hypoxic ADSC-derived exosomes enhance wound healing in diabetic mice via delivery of circ-Snhg11 and induction of M2-like macrophage polarization, *Biomed. Pharmacother.* 153 (2022), 113463.
- [17] W. Li, L. Zhang, B. Guo, Exosomal FMR1-AS1 facilitates maintaining cancer stem-like cell dynamic equilibrium via TLR7/NF κ B/c-Myc signaling in female esophageal carcinoma, *Mol. Cancer* 18 (2019) 22.
- [18] A. Yu, L. Zhao, Q. Kang, Transcription factor HIF1 α promotes proliferation, migration, and invasion of cholangiocarcinoma via long noncoding RNA H19/microRNA-612/Bcl-2 axis, *Transl. Res.* 224 (2020) 26–39.
- [19] C.Y. Liu, Y.H. Zhang, R.B. Li, LncRNA CAIF inhibits autophagy and attenuates myocardial infarction by blocking p53-mediated myocardium transcription, *Nat. Commun.* 9 (2018) 29.
- [20] J. Zhang, S. Li, L. Li, Exosome and exosomal microRNA: trafficking, sorting, and function, *Dev. Reprod. Biol.* 13 (2015) 17–24.
- [21] B. Li, S. Luan, J. Chen, The MSC-derived exosomal lncRNA H19 promotes wound healing in diabetic foot ulcers by upregulating PTEN via MicroRNA-152-3p, *Mol. Ther. Nucleic Acids* 19 (2020) 814–826.
- [22] Z.F. Han, J.H. Cao, Z.Y. Liu, Exosomal lncRNA KLF3-AS1 derived from bone marrow mesenchymal stem cells stimulates angiogenesis to promote diabetic cutaneous wound healing, *Diabetes Res. Clin. Pract.* 183 (2022), 109126.
- [23] M. Hu, Y. Wu, C. Yang, Novel long noncoding RNA lnc-URIDS delays diabetic wound healing by targeting Plod1, *Diabetes* 69 (2020) 2144–2156.
- [24] X. Liu, Y. Yang, Y. Li, Integration of stem cell-derived exosomes with in situ hydrogel glue as a promising tissue patch for articular cartilage regeneration, *Nanoscale* 9 (2017) 4430–4438.
- [25] O. Goor, S.I.S. Hendrikse, P.Y.W. Dankers, From supramolecular polymers to multi-component biomaterials, *Chem. Soc. Rev.* 46 (2017) 6621–6637.

- [26] Y. Ju, Y. Hu, P. Yang, Extracellular vesicle-loaded hydrogels for tissue repair and regeneration, *Mater. Today Bio.* 18 (2023), 100522.
- [27] P. Pleguezuelos-Beltrán, P. Gálvez-Martín, D. Nieto-García, Advances in spray products for skin regeneration, *Bioact. Mater.* 16 (2022) 187–203.
- [28] Y. Li, L. Li, Y. Li, Enhancing cartilage repair with optimized supramolecular hydrogel-based scaffold and pulsed electromagnetic field, *Bioact. Mater.* 22 (2023) 312–324.
- [29] W. Yuan, H. Wang, C. Fang, Microscopic local stiffening in a supramolecular hydrogel network expedites stem cell mechanosensing in 3D and bone regeneration, *Mater. Horiz.* 8 (2021) 1722–1734.
- [30] X. Xie, L. Hu, B. Mi, Metformin alleviates bone loss in ovariectomized mice through inhibition of autophagy of osteoclast precursors mediated by E2F1, *Cell Commun. Signal.* 20 (2022) 165.
- [31] P.J. Murray, Macrophage polarization, *Annu. Rev. Physiol.* 79 (2017) 541–566.
- [32] X. Liao, N. Sharma, F. Kapadia, Krüppel-like factor 4 regulates macrophage polarization, *J. Clin. Invest.* 121 (2011) 2736–2749.
- [33] J. Yan, G. Tie, S. Wang, Diabetes impairs wound healing by Dnmt1-dependent dysregulation of hematopoietic stem cells differentiation towards macrophages, *Nat. Commun.* 9 (2018) 33.
- [34] J. Qu, X. Zhao, Y. Liang, Antibacterial adhesive injectable hydrogels with rapid self-healing, extensibility and compressibility as wound dressing for joints skin wound healing, *Biomaterials* 183 (2018) 185–199.
- [35] K. Huang, W. Liu, W. Wei, Photothermal hydrogel encapsulating intelligently bacteria-capturing bio-MOF for infectious wound healing, *ACS Nano* 16 (2022) 19491–19508.
- [36] I. Vanni, A. Alama, F. Grossi, Exosomes: a new horizon in lung cancer, *Drug Discov. Today* 22 (2017) 927–936.
- [37] Y. Wang, Z. Cao, Q. Wei, VH298-loaded extracellular vesicles released from gelatin methacryloyl hydrogel facilitate diabetic wound healing by HIF-1 α -mediated enhancement of angiogenesis, *Acta Biomater.* 147 (2022) 342–355.
- [38] N. Hu, Z. Cai, X. Jiang, Hypoxia-pretreated ADSC-derived exosome-embedded hydrogels promote angiogenesis and accelerate diabetic wound healing, *Acta Biomater.* 157 (2023) 175–186.
- [39] Y. Gao, Z. Yuan, X. Yuan, Bioinspired porous microspheres for sustained hypoxic exosomes release and vascularized bone regeneration, *Bioact. Mater.* 14 (2022) 377–388.
- [40] L. Ge, C. Xun, W. Li, Extracellular vesicles derived from hypoxia-preconditioned olfactory mucosa mesenchymal stem cells enhance angiogenesis via miR-612, *J. Nanobiotechnol.* 19 (2021) 380.
- [41] F. Ferrè, A. Colantoni, M. Helmer-Gitterich, Revealing protein-lncRNA interaction, *Briefings Bioinf.* 17 (2016) 106–116.
- [42] E. Dangelmaier, A. Lal, Adaptor proteins in long noncoding RNA biology, *Biochim. Biophys. Acta Gene Regul. Mech.* 1863 (2020), 194370.
- [43] De Bramblett, N.G. Copeland, N.A. Jenkins, BHLHB4 is a bHLH transcriptional regulator in pancreas and brain that marks the dimesencephalic boundary, *Genomics* 79 (2002) 402–412.
- [44] K. Aviña-Padilla, J.A. Ramírez-Rafael, G.E. Herrera-Oropeza, Evolutionary perspective and expression analysis of intronless genes highlight the conservation of their regulatory role, *Front. Genet.* 12 (2021), 654256.
- [45] X. Yang, B.J. Mathis, Y. Huang, KLF4 promotes diabetic chronic wound healing by suppressing Th17 cell differentiation in an MDSC-dependent manner, *J. Diabetes Res.* 2021 (2021), 7945117.